

Hydrothermal synthesis of WO₃ nanorods: structure, growth and gas sensing properties

SHIXIU CAO, HUI CHEN*

Research institute for new material technology, Chongqing University of Arts and Science, Chongqing, 402160, China

Unique WO₃ nanorods were synthesized successfully via a novel one-step hydrothermal method with the assistance of potassium sulfate (K₂SO₄). The WO₃ nanorods had uniform size with diameters around 30 nm and length up to 100~250nm. Moreover, it was surprisingly noticed that the K₂SO₄ played a key factor on fabrications of WO₃ nanorods. A possible growth mechanism of the WO₃ nanorods was also proposed. We found that the WO₃ nanorods showed excellent gas sensing performances towards ethanol. The facile preparation method and the improved properties derived from the one-dimensional structures of nanorods are significant in the synthesis and future applications of functional nanomaterials.

(Received April 27, 2018; accepted November 29, 2018)

Keywords: WO₃, Hydrothermal, Microstructure, Crystal growth, Sensors

1. Introduction

As an n-type metal oxide semiconductor, tungsten oxide (WO₃) nanomaterials have attracted special attention due to its promising physical and chemical properties [1-2]. We all know that the morphological characteristics of the nanomaterials such as grain size and structure play a crucial role in affecting their chemical and physical properties [3-8]. The one-dimensional (1D) WO₃ nanomaterials with a large surface area, show many outstanding properties, such as gas sensors, photocatalysts, field-emission devices, and solar-energy devices [9-12]. Therefore, many methods have been developed to synthesize 1D WO₃ nanostructures, such as thermal evaporation, solid-state, sol-gel and solution-based colloidal method [13-16]. Thereinto, as a facile method, hydrothermal processes in the presence of some inorganic salt solution have also been applied for the preparation of 1D WO₃ nanostructures. Recently, a great deal of effort has been focused on the hydrothermal synthetic routes of 1D WO₃ nanostructures such as nanowires, nanorods, nanotubes [17-19], and so on. However, the most of researches still focuses on the synthesis of the 1D WO₃ nanostructures, and there is still no deep understanding of the growth and gas sensing mechanism of 1D WO₃ nanostructures that can be widely accepted.

In present work, controlled morphology and growth mechanism of WO₃ nanorods were carried out by a facile hydrothermal route with the assistance of potassium sulfate. Furthermore, the gas-sensing performances of the as-prepared WO₃ nanorods were investigated towards ethanol.

2. Experimental

Synthesis of sample: All the chemical reagents were of analytical grade and used directly without further purification. Firstly, sodium tungstate (Na₂WO₄·2H₂O) (0.005Mol), and potassium sulfate (K₂SO₄) (0.01Mol), 0.12g citric acid were dissolved in 50ml deionized water under the continual stirring. Afterwards, pH value of the obtained solution was adjusted to 1.3~1.5 by adding 2mol/L hydrochloric acid (HCl). The final solution was transferred into a 100 ml Teflon-lined stainless steel autoclave, and sealed, heated in oven at 130 °C for 12 h. Then the precursor was collected by centrifugation, and washed several times with distilled water and absolute ethanol. Finally, the as-prepared sample was dried in air at 300 °C for 4 h.

Characterization of sample: The crystal structure of the as-prepared samples was characterised by X-Ray Diffraction (XRD), a Rigaku D/Max-1200X diffractometry equipped with Cu K α radiation. The morphologies and microstructures were analyzed by scanning electron microscopy (FE-SEM, Nova 400 Nano) and transmission electron microscope (TEM, ZEISS, LIBRA 200). The gas sensing properties were measured with HW-30 A gas sensitivity instrument (Hanwei Electronics Co., Ltd.)

Fabrication of the gas sensor: Firstly, the as-prepared WO₃ power was dispersed in distilled water to form paste. Next, the formed turbid liquid was then spin coated onto an alumina ceramic tube, positioned with a pair of Au electrodes and four Pt wires at each end point. In order to control the operating temperature, the Ni-Cr wire was inserted into the alumina tube as a heater. The schematic of the gas sensor is shown in Fig. 1. Finally, the gas sensor was dried at 350 °C for 3 h to evaporate the existed organic binder.

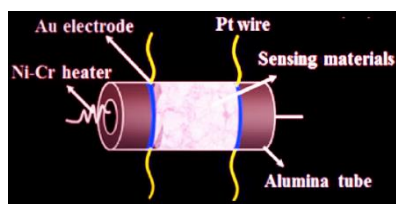


Fig. 1. Schematic diagrams of the gas sensor

3. Results and discussion

3.1. XRD analysis

The XRD patterns of the precursor and as-prepared product are showed in Fig. 2. As shown in Fig. 2a, we can see that all the observed reflection peaks of the precursor can be indexed to the $\text{WO}_3 \cdot \text{H}_2\text{O}$, and agree well with the standard data file (JCPDS no. 44-0363). The high and sharp peaks show that $\text{WO}_3 \cdot \text{H}_2\text{O}$ is with good crystallinity in the precursors. The XRD pattern of the as-prepared products is shown in Fig. 2(b). No other peaks can be observed from this pattern, which indicates a pure hexagonal WO_3 (JCPDS no. 75-2187, $a=b=0.7298$ nm, $c=0.3899$ nm). In addition, the narrow and strong peaks illustrate the high crystallinity of the obtained h-WO_3 products.

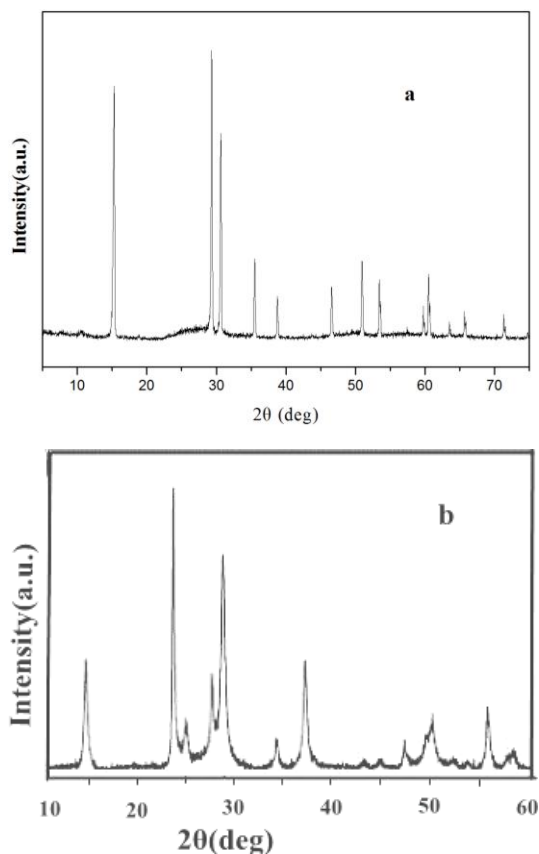


Fig. 2. XRD patterns of the precursors (a) and as-prepared product (b)

3.2. SEM observation

The morphologies and structure of the obtained products were investigated by SEM and TEM. The SEM images for this product were shown in Fig. 3a-c, from which we could see that there existed a mount of nanorods with diameters around 30 nm and length up to 100~250 nm. The detailed observation and characterization on the morphology and structure was carried out using TEM, HRTEM and SAED, as shown in Fig. 3d-f. TEM image (Fig. 3d) of an individual nanorod showed that it was about 25 nm in diameter and 100 nm in length. Its HRTEM image (Fig. 3e and f) displayed a regular spacing of the lattice fringes, which were found to be about 0.316 nm and 0.389 nm, corresponding to the (200) planes and (001) planes of h-WO_3 , respectively. Moreover, we could see in Fig. 3e that the lattice fringes of (200) plane along c-axis, were perpendicular to another fuzzy lattice fringes of (001) plane. The result indicated that the single WO_3 nanorod grew along the [001] directions and with the exposure of planes (200).

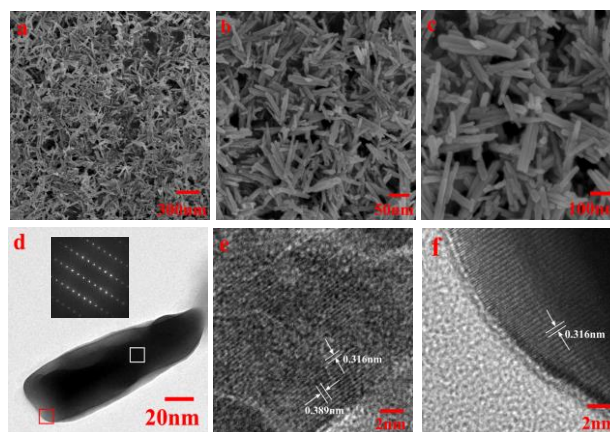


Fig. 3. SEM (a-c), TEM (d), (inset) SAED, (e-f) HRTEM images of the h-WO_3 nanorods

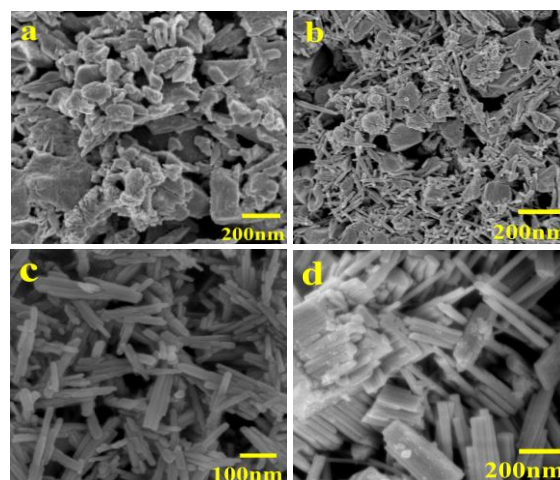


Fig. 4. SEM images of the as-prepared WO_3 products with different K_2SO_4 concentrations: (a) 0 Mol, (b) 0.005 Mol, (c) 0.01 Mol, (d) 0.015 Mol

To gain insight into the formation mechanism of the WO₃ nanorods and how morphology evolves with processing conditions, we have performed a straightforward comparative investigation by adjusting the different K₂SO₄ concentrations under the same reaction condition, as shown in Fig. 4. We could see that there was only irregular aggregation obtained without K₂SO₄. Whereas, addition of 0.005 M K₂SO₄ led to mixed morphologies consisting of irregular particles and nanorods. The particles were with diameter of 200 nm, and the nanorods were with about 25 nm in diameter and 100 nm in length. The result indicated that K₂SO₄ could promote the formation of nanorods. When the K₂SO₄ concentration was enhanced to 0.01 M, well-defined nanorods with diameter of 30 nm and length of 100~250 nm (Fig. 4c) can be obtained. Along with the concentration of K₂SO₄ further increasing up to 0.015 M, the obtained nanorods started to form the aggregation of nanorods with the diameters around 30 nm and length up to 200~400 nm. So, we could see that a suitable K₂SO₄ concentration can promote the crystal growing along its [001] crystal direction (c-axis) to form the nanorod, upon enhancing the K₂SO₄ concentrations from 0 to 0.015 M as shown in Fig. 4.

3.3. Growth mechanism

On the basis of the above experimental results, we proposed a possible growth mechanism for the formation of the WO₃ nanorods, as shown in Fig. 5. In our

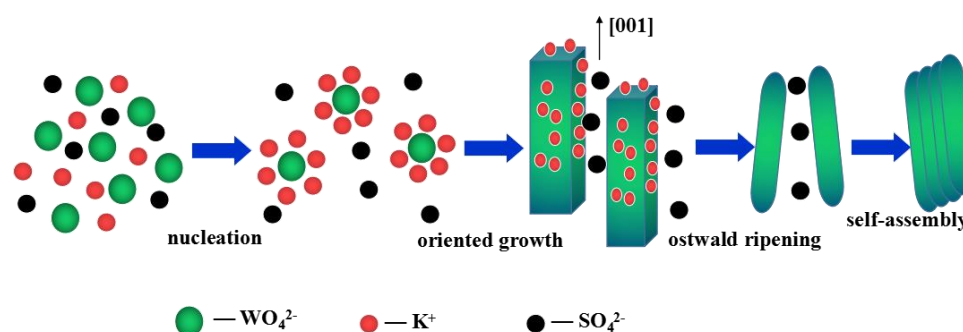
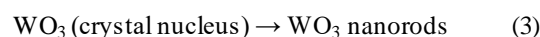
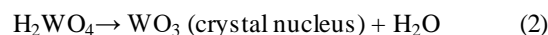


Fig. 5. Schematic model of the formation mechanism of WO₃ nanorods

3.4. Gas-sensing properties

Gas sensing properties of the four WO₃ nanostructures fabricated sensors were measured to gain insight into the gas sensing properties of the WO₃ nanorods, as shown in Fig. 6. Firstly, the sensors were tested at different heating temperature from 200°C to 450°C. From Fig. 6A, we could

experiment, firstly Na₂WO₄ and HCl reacted with each other to form H₂WO₄. The WO₃ crystal nucleus was obtained at the beginning of the hydrothermal reaction. The reaction routes for the synthesis of WO₃ nanorods could be expressed as follows:



The formation and evolution processes of the WO₃ nanorods seem to be divided into three steps: initial nucleation process (WO₃ crystal nucleus), short rod-like nanostructures formation (oriented aggregation), and self-assembly process (Ostwald ripening). At the initial stage of hydrothermal treatment, because high concentration was suitable for the rapid formation of small crystallites, WO₃ crystal nucleus formed, and numerous WO₃ nanoparticles were produced due to the domination of kinetic factor. Due to the induction action of Na⁺ and K⁺, the primary WO₃ nanoparticles grew along [001] direction, with the hydrothermal time prolonging. So, these primary particles would continuously grow into nanorods due to the different growth energy of the (001) and (100) faces. With the increase of the K₂SO₄ concentrations, the absorption action of SO₄²⁻ ions would promote the constructing of the single nanorods into the nanorods bundles.

see that the highest gas responses for the WO₃ products (a–d) to the ethanol were estimated to be 33, 45, 61 and 47, respectively. So, the sensor based on WO₃ nanorods (c) exhibited higher response compared with the other sensors, which indicated the morphology of nanorods was critical to further enhance gas sensing properties of WO₃.

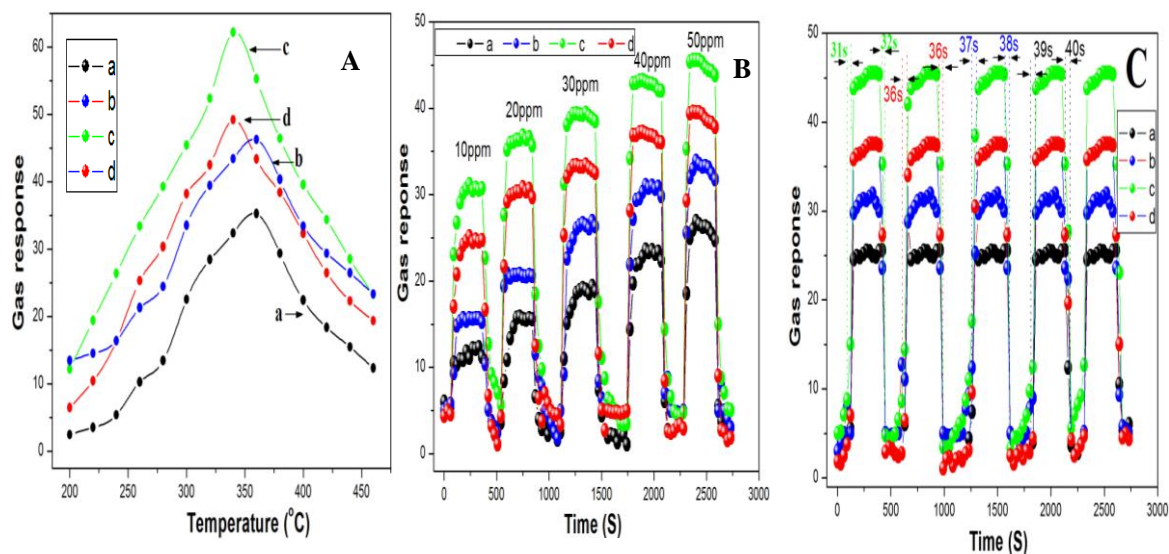


Fig. 6. (A) Response of the as-prepared WO_3 products with different K_2SO_4 concentrations (a: 0 Mol, b: 0.005 Mol, c: 0.01 Mol, d: 0.015 Mol) vs heating temperature of the sample to 100 ppm ethanol. (B) Response of the as-prepared WO_3 products at different concentration of ethanol at 350°C . (C) The consistent response and recovery characteristics of the as-prepared WO_3 sensors throughout the five cyclic tests to the ethanol gas of 50 ppm at 350°C

Furthermore, we measured the response of the four samples to ethanol under the different concentrations at 350°C . As shown in Fig. 6B, the gas response of the four samples increased with the rise of gas concentration. Moreover, the WO_3 nanorods (c) sensor exhibited higher response than others, which further implied that the WO_3 nanorods might play an important role in improving the gas sensing performances.

Finally, the gas response and recovery behavior of all the samples to 50 ppm at 350°C was measured. The results are shown in Fig. 6C. Five reversible cycles of the response and recovery curves indicated a stable and repeatable characteristic. Furthermore, the response/recovery time of the WO_3 nanorods (c) was ~ 31 s/32 s. As for the samples (d), slightly prolonged response/recovery behavior was ~ 36 s/36 s. The response and recovery times were estimated to be 37 s and 38 s, respectively, for the samples (b). The response/recovery time of the samples (a) was 42 s/42 s. The WO_3 nanorods (c) sensor exhibited higher gas response than the other samples (a, b, d).

Therefore, based on the above experimental results and analysis, we could find that the WO_3 nanorods had the significant effect on gas response improvement, and the WO_3 nanorods sensor had excellent selectivity to ethanol and good stability.

4. Conclusions

We have successfully synthesized the WO_3 nanorods via the simple yet facile hydrothermal method. We

discussed in detail the possible growth mechanism of the WO_3 nanorods. Moreover, the WO_3 nanorods showed the excellent gas sensing properties toward ethanol. The response of sensor to ethanol gas strongly depended on the structure and morphology of as-synthesized WO_3 nanorods. The results demonstrate that this unique morphology holds substantial promise for the use of WO_3 as a gas sensing material in future sensor applications.

Acknowledgements

The authors acknowledge the financial support to this work from the Basic and Frontier Research Program of Chongqing Municipality (cstc2016jcyjA0567, cstc2017jcyjBX0051), the Science and Technology Research Program of Chongqing Municipal Education Commission (KJ1711282, KJ1711283), the open project of Key Lab of Advanced Materials of Yunnan Province (2016cx06), the Natural Science Foundation of China (51702033).

References

- [1] J. Su, X. Feng, J. D. Sloppy, L. Guo, C. A. Grimes, *Nano Lett.* **11**(1), 203 (2011).
- [2] D. Chen, J. Ye, *Adv. Funct. Mater.* **18**(13), 1922 (2008).
- [3] L. Wang, J. Zhan, W. Fan, G. Cui, H. Sun, L. Zhuo, et al., *Chem. Commun.* **46**(18), 8833 (2010).
- [4] Z. Gu, H. Li, T. Zhai, W. Yang, Y. Xia, Y. Ma, et al., *J.*

- Solid State Chem. **180**(1), 98 (2007).
- [5] Z. C. Wang, M. Saito, K. P. McKenna, et al., *Nano. Lett.* **3**(16), 1530 (2016).
- [6] H. W. Long, W. Zeng, H. Wang, et al., *Adv. Sci.* **5**, 3 (2018).
- [7] Z. C. Wang, M. Saito, K. P. McKenna, et al., *Nature* **7373**(479), 380 (2011).
- [8] R. Sun, Z. C. Wang, M. Saito, N. Shibata, Y. C. Ikuhara, *Nat. Commun.* **6**(7120), 6 (2015).
- [9] H. L. Zhang, Z. F. Liu, J. Q. Yang, W. Guo, L. J. Zhu, W. J. Zheng, *Mater. Res. Bull.* **57**(23), 260 (2014).
- [10] Q. Xiang, G. F. Meng, H. B. Zhao, Y. Zhang, H. Li, W. J. Ma, *J. Phys. Chem. C* **114**(5), 2049 (2010).
- [11] A. Yella, U. K. Gautam, E. Mugnaioli, M. Panthofer, Y. Bando, D. Golberg, *Cryst. Eng. Comm.* **13**(12), 4074 (2011).
- [12] A. Yan, C. Xie, D. Zeng, S. Cai, M. Hu, *Mater. Res. Bull.* **45**(10), 1541 (2010).
- [13] S. J. Wang, W. J. Lu, G. Cheng, K. Cheng, X. H. Jiang, Z. L. Du, *Appl. Phys. Lett.* **94**, 263106-1 (2009).
- [14] Y. Wu, Z. H. Xi, G. M. Zhang, J. Yu, D. Z. Guo, *J. Cryst. Growth* **292**(1), 143 (2006).
- [15] Z. J. Gu, Y. Ma, W. S. Yang, G. J. Zhang, J. N. Yao, *Chem. Commun.* **28**, 3597 (2005).
- [16] L. F. Chen, X. T. Zhang, Y. H. Chen, B. Liu, Y. C. Li, Y. B. Huang, Z. L. Du, *Chin. J. Inorg. Chem.* **20**(9), 1117 (2004).
- [17] L. Gao, X. F. Wang, Z. Xie, W. F. Song, L. J. Wang, X. Wu, F. Y. Qu, D. Chen, G. Z. Shen, *J. Mater. Chem. A* **1**(24), 7167 (2013).
- [18] F. Zheng, M. Zhang, M. Guo, *Thin Solid Films* **534**, 45 (2013).
- [19] J. Li, X. Liu, Q. Han, X. Yao, X. Wang, *J. Mater. Chem. A* **1**(4), 1246 (2013).

*Corresponding author: 18580872389@163.com